Available online at www.sciencedirect.com
SCIENCE DIRECT
Journal of Colloid and Interface Science 285 (2005) 627–633
JOURNAL OF Colloid and Interface Science
www.elsevier.com/locate/jcis

Hydrodynamics of an ideal aggregate with quadratically increasing permeability

Albert S. Kim *, Rong Yuan

Civil and Environmental Engineering, University of Hawaii at Manoa, 2540 Dole Street, Honolulu, HI 96822, USA

Received 8 September 2004; accepted 1 December 2004

Available online 18 January 2005

Abstract

In this study, we consider the ideal aggregate with quadratically increasing permeability $\kappa = k_2 r^2$ and derive the analytical expression of the stream function within the porous aggregate by incorporating the Brinkman and continuity equations. The hydrodynamic properties of the aggregate are investigated by taking account of the hydrodynamic radius, settling velocity, and fluid collection efficiency, which are found to be solely dependent on the permeability prefactor k_2. The fractal dimension D_f and prefactor k_2 of the ideal aggregate are found to be $5/3$ (=1.67) and 0.20, respectively, and well describe the hydrodynamics of aggregates formed in the diffusion-limited-cluster-aggregation (DLCA) regime. More important, hydrodynamic similarity between the ideal aggregate and impermeable solid sphere is discovered in terms of variations of the hydrodynamic radius, settling velocity, and fluid collection efficiency with respect to the aggregate radius.

Keywords: Aggregation; Fractal aggregate; Permeability; Settling velocity; Hydrodynamic radius

1. Introduction

A key element to understanding the dynamics of colloidal motion in the environment and in engineered systems is an accurate depiction of the underlying mechanics driving the transport behavior. In general, colloidal motion will entail complications that arise when colloids coalesce to form aggregate structures with spatially varying porosities within them. In such cases, the variable porosities translate into complex flow fields for fluid both penetrating into and circumventing around the aggregate. Accurate description of this flow dynamic represents an important advancement in the study of colloidal motion involving aggregation. In this paper, we present an effective method of capturing the flow field within an aggregate structure by recasting the aggregate shape as a hydrodynamically equivalent porous sphere with quadratically increasing permeability from its core.

A plethora of fundamental research has been focused on the mechanisms responsible for the aggregation of colloids [1,2], but only relatively few studies have addressed the equally important subject of the hydrodynamic properties of the aggregate after it has been formed [3–5]. Johnson et al. [6] present a good initial approach for modeling an aggregate as a uniformly porous sphere using the Brinkman equation with constant permeability. However, this method is unsatisfactory, as it tends to overestimate the hydrodynamic radius, and thus consequently underestimate the inversely proportional aggregate settling velocity. In a real aggregate, the porosity within it varies radially from a dense core to sparse outer edges. The highly porous outer edges allow for more fluid flow to penetrate into the inner regions of the aggregate compared to the case of a uniformly porous sphere of the same mass. With greater amounts of fluid flow through it, the aggregate will experience less hydrodynamic drag and thus settle faster than its constant porosity counterpart. Furthermore, the primary particles that form the aggregate are not uniformly distributed around the outer edges, but rather, are either clumped locally or branched into tree-like struc-

* Corresponding author. Fax: +1(808)956-5014.
E-mail address: albertsk@hawaii.edu (A.S. Kim).

0021-9797/$ – see front matter
doi:10.1016/j.jcis.2004.12.009

tures [7,8]. This is due to the full connectivity of all primary particles within the aggregate (even in the highly porous regions). Therefore, the intermediate void spaces among local groups of primary particles will also experience lower hydrodynamic drag.

In light of this, recasting the aggregate by a hydrodynamically equivalent fractal structure of radially varying permeability appears to be a more representative description. Some measurable steps toward this goal have been accomplished beginning with Ooms et al. [9] who provide confirmation of Brinkman's analytic expression as the solution of the hydrodynamic radius of a sphere with constant inner permeability [10,11]. Veerapaneni and Wiesner [4] use the stream functions for uniformly porous spheres, apply boundary conditions stipulating continuous velocity and stress fields between adjacent shells, and then numerically calculate the hydrodynamic radius and fluid collection efficiency. The improvement of their model is only limited as Vanni [12] later proves that the method of Veerapaneni and Wiesner [4] is valid only for aggregates of fractal dimension greater than 2.1.

Due to its mathematical complexity, the complete solution to the Brinkman equation with a continuous and variable permeability has not been found yet. And so, in this paper, we present a critical advancement in the modeling of ideal fractal aggregates by solving the Brinkman equation for a porous sphere with quadratically increasing permeability from its core. The hydrodynamic properties of the sphere of variable permeability are investigated and compared to those of impermeable spheres.

2. Theory

Our model is an isolated ideal aggregate of outer radius R, experiencing a uniform upward flow V, as shown in Fig. 1. Relative to the ideal aggregate, the creeping flow of Newtonian fluid with absolute viscosity μ is considered to be steady and axi-symmetric, and for mathematical convenience the center of the ideal aggregate is selected as the origin of the spherical coordinates (r, θ, φ).

The internal permeability of the aggregate is quadratically increasing with respect to distance from the center of the aggregate in a radial direction:

$$\kappa = k_2 r^2, \tag{1}$$

where k_2 is a permeability prefactor, which is a pure number because the permeability has a physical dimension of length squared.

2.1. Governing equations

The incompressible Newtonian flow exterior to the aggregate is described by the Stokes and continuity equations as

$$\mu \nabla^2 u = \nabla p \tag{2}$$

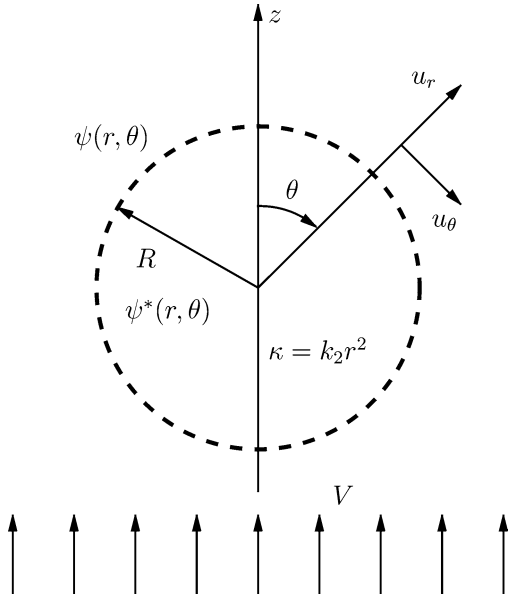

Fig. 1. Coordinate system for axi-symmetric flow relative to an isolated ideal aggregate with quadratically increasing permeability.

and

$$\nabla \cdot u = 0, \tag{3}$$

respectively, where u $(= [u_r, u_\theta, u_\varphi])$ is the fluid velocity vector and p is the fluid pressure. Inside the aggregate, conservation of momentum is expressed by the Brinkman and continuity equations as

$$\mu^* \nabla^2 u^* - \frac{\mu^*}{\kappa} u^* = \nabla p^* \tag{4}$$

and

$$\nabla \cdot u^* = 0, \tag{5}$$

respectively, where * denotes any macroscopically averaged quantity pertaining specifically to the interior porous region of the aggregate. In this light, μ^* represents an effective viscosity within the porous aggregate but is often assumed identical to μ, especially where the porosity is high.

2.2. Boundary conditions

The physically realistic and mathematically consistent boundary conditions which describe the current problem are given as

$$\lim_{r\to 0} u_r^* \to \text{finite}, \tag{6}$$

$$\lim_{r\to 0} u_\theta^* \to \text{finite}, \tag{7}$$

$$u_r(R,\theta) = u_r^*(R,\theta), \tag{8}$$

$$u_\theta(R,\theta) = u_\theta^*(R,\theta), \tag{9}$$

$$\tau_{rr}(R,\theta) = \tau_{rr}^*(R,\theta), \tag{10}$$

$$\tau_{r\theta}(R,\theta) = \tau_{r\theta}^*(R,\theta), \tag{11}$$

$$\lim_{r\to\infty} u_r = V\cos\theta, \tag{12}$$

$$\lim_{r\to\infty} u_\theta = -V\sin\theta, \tag{13}$$

where $0 \leqslant \theta \leqslant 2\pi$ and $\tau_{rr}^{(*)}$ and $\tau_{r\theta}^{(*)}$ denote the normal and tangential components of the stress tensors of fluid flow, i.e.,

$$\tau_{rr}^{(*)} = -p^{(*)} + 2\mu^{(*)}\frac{\partial u_r^{(*)}}{\partial r} \tag{14}$$

and

$$\tau_{r\theta}^{(*)} = \mu^{(*)}\left(\frac{1}{r}\frac{\partial u_r^{(*)}}{\partial\theta} + \frac{\partial u_\theta^{(*)}}{\partial r} - \frac{u_\theta^{(*)}}{r}\right), \tag{15}$$

respectively, for both outside (unstarred) and inside (starred) the aggregate.

Equations (6) and (7) indicate the finitude of the velocity field at the center of the aggregate. Eqs. (8)–(11) point to the continuity of the normal and tangential components of velocity and stress tensor across the permeable interface, while Eqs. (12) and (13) show the uniformity of the velocity field far from the aggregate. With the incompressibility of the Newtonian fluid implied in Eqs. (3) and (5), it has been proven that the continuity of the normal stress (Eq. (10)) is equivalent to that of the fluid pressure [13,14]:

$$p^*(R,\theta) = p(R,\theta). \tag{16}$$

2.3. Solution

Independence of the flow on the azimuthal angle φ, i.e., axi-symmetry, introduces stream functions ψ and ψ^* related to the velocity fields by

$$u_r^{(*)} = \frac{-1}{r^2\sin\theta}\frac{\partial\psi^{(*)}}{\partial\theta} \tag{17}$$

and

$$u_\theta^{(*)} = \frac{1}{r\sin\theta}\frac{\partial\psi^{(*)}}{\partial r}, \tag{18}$$

where $0 \leqslant \theta \leqslant 2\pi$. Taking the curl of the Stokes equation (Eq. (2)) and the Brinkman equation (Eq. (4)), one can obtain

$$E^4\psi = 0, \quad r \geqslant R, \tag{19}$$

and

$$E^4\psi^* - \frac{1}{\kappa(r)}E^2\psi^* + \frac{1}{\kappa^2(r)}\frac{\partial\kappa(r)}{\partial r}\frac{\partial\psi^*}{\partial r} = 0, \quad 0 \leqslant r \leqslant R, \tag{20}$$

respectively, where

$$E^2 = \frac{\partial^2}{\partial r^2} + \frac{\sin\theta}{r^2}\frac{\partial}{\partial\theta}\left(\frac{1}{\sin\theta}\frac{\partial}{\partial\theta}\right) \tag{21}$$

with the macroscopic assumption of

$$\mu = \mu^*. \tag{22}$$

The general solution of Eq. (19) is well known as

$$\psi(\xi,\theta) = -\frac{1}{2}VR^2(A\xi^{-1} + B\xi + C\xi^2 + D\xi^4)\sin^2\theta \tag{23}$$

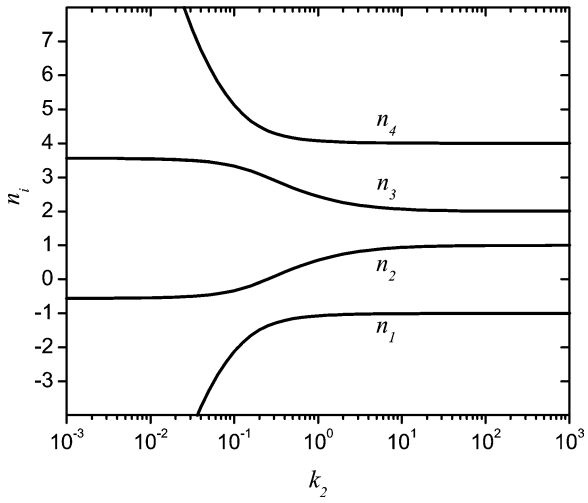

Fig. 2. Variation of the exponent n_i ($i = 1, 2, 3$, and 4) of Eq. (25) with the permeability prefactor k_2.

and that of Eq. (20) with Eq. (1) is derived in this paper as

$$\psi^*(\xi,\theta) = -\frac{1}{2}VR^2(E\xi^{n_1} + F\xi^{n_2} + G\xi^{n_3} + H\xi^{n_4})\sin^2\theta, \tag{24}$$

where $\xi = r/R$. The four exponents of n_i ($i = 1, 2, 3$, and 4) are given as

$$\begin{aligned}
n_1 &= \frac{3}{2} - \frac{1}{2}\sqrt{13 + \frac{2}{k_2} + 2\sqrt{36 - \frac{4}{k_2} + \frac{1}{k_2^2}}},\\
n_2 &= \frac{3}{2} - \frac{1}{2}\sqrt{13 + \frac{2}{k_2} - 2\sqrt{36 - \frac{4}{k_2} + \frac{1}{k_2^2}}},\\
n_3 &= \frac{3}{2} + \frac{1}{2}\sqrt{13 + \frac{2}{k_2} - 2\sqrt{36 - \frac{4}{k_2} + \frac{1}{k_2^2}}},\\
n_4 &= \frac{3}{2} + \frac{1}{2}\sqrt{13 + \frac{2}{k_2} + 2\sqrt{36 - \frac{4}{k_2} + \frac{1}{k_2^2}}},
\end{aligned} \tag{25}$$

and their sole dependence on the permeability prefactor k_2 is shown in Fig. 2. The accuracy of Eq. (25) can be proven by taking the limit as $k_2 \to \infty$ (i.e., void space): the exponents n_1, n_2, n_3, and n_4 respectively reach -1, 1, 2, and 4, which are identical to the four exponents of ξ of Eq. (23). Chernyakov [5] performed similar calculations, but he obtained only two terms with the exponents of n_3 and n_4 in Eq. (24).

In order to satisfy the required set of boundary conditions stipulated in Eqs. (6)–(13), the arbitrary constants A, B, C, D, E, F, G, and H appearing in the stream functions of Eqs. (23) and (24) are specified as

$$A = +\frac{1}{2}\frac{[(n_3-1)(n_3-2)(n_4-1)(n_4-2)k_2 + n_3n_4 - 2]}{J}, \tag{26}$$

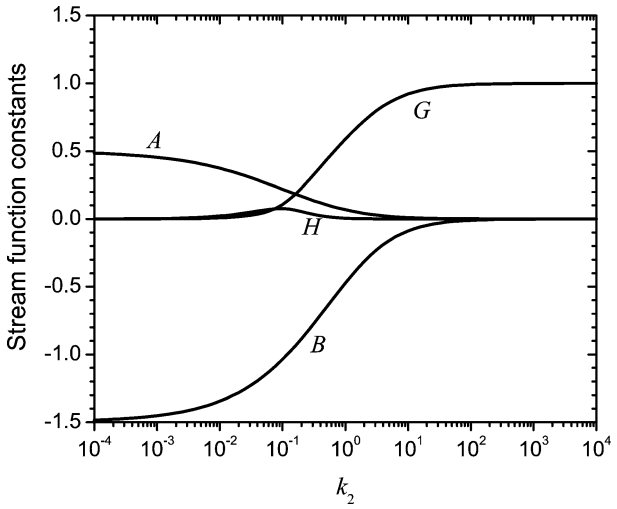

Fig. 3. Variation of the stream function constants A, B, G, and H of Eqs. (23) and (24) with the permeability prefactor k_2.

$$B = -\frac{3}{2}\frac{[(n_3+1)(n_3-2)(n_4+1)(n_4-2)k_2 + n_3 n_4 + 2]}{J}, \tag{27}$$

$$C = 1, \tag{28}$$

$$D = 0, \tag{29}$$

$$E = 0, \tag{30}$$

$$F = 0, \tag{31}$$

$$G = +\frac{3[(n_4-1)(n_4-2)(n_4+1)k_2 - n_4]}{(n_4-n_3)J}, \tag{32}$$

$$H = -\frac{3[(n_3-1)(n_3-2)(n_3+1)k_2 - n_3]}{(n_4-n_3)J}, \tag{33}$$

where

$$J = (n_3+1)(n_3-1)(n_4+1)(n_4-1)k_2 + n_3 n_4 + 1. \tag{34}$$

Fig. 3 shows the dependence of A, B, G, and H on the permeability prefactor k_2. It is worth noting that A, B, and H converge to zero and G becomes one in the limit of $k_2 \to \infty$, indicating

$$\psi = \psi^* \to -\frac{V R^2}{2}\xi^2, \tag{35}$$

which is the stream function of the uniform ambient flow in the absence of the ideal aggregate.

Integrating the normal and tangential stress distributions over the porous surface yields the drag force exerted on the ideal aggregate as

$$\mathbf{F} = 2\pi R^2 \int_0^\pi [\tau_{rr}\cos\theta - \tau_{r\theta}\sin\theta]_{r=R}\sin\theta\,\mathrm{d}\theta = 6\pi\mu V R\Omega, \tag{36}$$

where

$$\Omega = -\frac{2}{3}B. \tag{37}$$

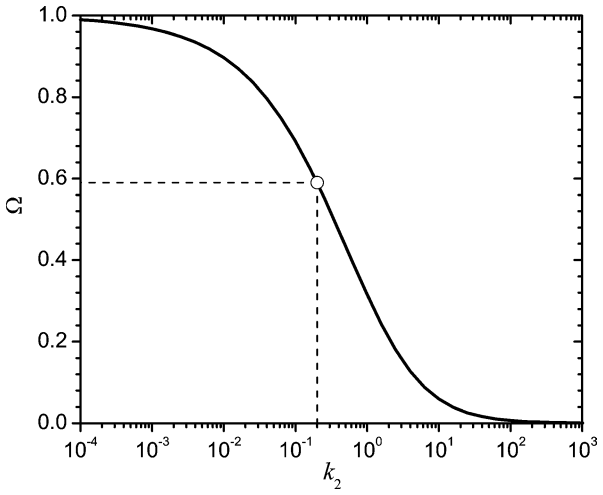

Fig. 4. Variation of the dimensionless hydrodynamic drag force Ω with the permeability prefactor k_2. The hollow circle signifies $\Omega = 0.59$ with $k_2 = 0.20$ of the DLCA aggregate (see Section 3.1 for details).

The physical meaning of Eq. (37) is the ratio of hydrodynamic resistance experienced by a porous sphere of radius R to that exerted on an impermeable sphere of the same radius. Then, the hydrodynamic radius of the aggregate can be defined as

$$R_h = R\Omega, \tag{38}$$

so that Ω is considered as a dimensionless hydrodynamic radius or drag force. The negative sign in Eq. (37) refers to the direction of the mechanical force $(-z)$ that sustains the ideal aggregate in the upward ambient fluid flow. Fig. 4 shows the variation of the dimensionless hydrodynamic drag force Ω as a sole function of the permeability prefactor k_2. As k_2 tends to zero, Ω converges to one, which implies that the ideal aggregate becomes an impermeable solid sphere. On the other hand, as k_2 diverges to infinity, Ω vanishes, which indicates the absence of the aggregate in the ambient flow field.

3. Results and discussion

3.1. Settling velocity and hydrodynamic radius

The number of primary particles N within an aggregate scales with the outer radius R and the gyration radius R_g, i.e.,

$$N = k_f\left(\frac{R}{a_p}\right)^{D_f} \tag{39}$$

and

$$N = k_0\left(\frac{R_g}{a_p}\right)^{D_f}, \tag{40}$$

respectively. Here, D_f is a fractal dimension, and k_f and k_0 are prefactors of Eqs. (39) and (40), respectively. Equa-

tion (39) then provides a radial solid fraction profile, i.e.,

$$\phi(r) = \frac{1}{3} k_f D_f \left(\frac{r}{a_p}\right)^{D_f - 3}, \tag{41}$$

which affords a relationship between the outer radius and the gyration radius as follows:

$$R_g = R\sqrt{\frac{D_f}{D_f + 2}}. \tag{42}$$

Then, substitution of Eq. (42) into Eq. (40) and equating Eqs. (39) and (40) renders k_f represented by k_0 as follows:

$$k_f = k_0 \left(\frac{D_f}{D_f + 2}\right)^{D_f/2}. \tag{43}$$

A specific permeability expression as a function of solid fraction is required to link the ideal aggregate of quadratically increasing permeability to a fractal aggregate that can be characterized with Eqs. (39)–(43). Most fractal aggregates, especially those with a fractal dimension that is less than 2, have a tree-like branched structure [7,8]. Hence, the permeability expression for fibrous porous media [15] is appropriate for the highly porous fractal aggregate. Permeability expressions for uniformly porous media composed of monodispersed spheres, however, do not reflect the complete connectivity of the spheres within the porous aggregates. In this light, we adopt Davies' empirical permeability correlation [15] and approximate the expression for a low solid volume fraction as follows:

$$\kappa_D = \frac{a_p^2}{16\phi^{1.5}(1 + 56\phi^3)} \approx \frac{a_p^2}{16}\phi^{-3/2}. \tag{44}$$

The validity of the approximation in Eq. (44) can be confirmed if the volume fraction is of an order of 0.1 or less, based on negligence of the ϕ^3 term in the denominator. The core region of the fractal aggregate typically has a volume fraction greater than 0.1, and so the approximation of Eq. (44) can be questionable in the central region. However, volume occupied by the core region is in general highly negligible compared to that of the edge region where most fluid flow can easily pass through. Therefore, Eq. (44) can be readily adopted in general as the permeability expression of the aggregate of the tree-like fractal structure with tolerable error from the aggregate core.

Substituting Eq. (41) into Eq. (44) and equating Eqs. (1) and (44) provide a relationship between k_2 and k_f, given as

$$k_2 = \frac{27}{16}(5k_f)^{-3/2}, \tag{45}$$

and a fractal dimension value of the ideal aggregate, given as

$$D_f = 3 + 2(-3/2)^{-1} = 5/3 = 1.67. \tag{46}$$

In Eq. (46), 3 is from the three-dimensional Euclidean space, 2 is from the quadratic permeability of Eq. (1), and $-3/2$ is from the exponent of ϕ in Davies' permeability correlation of Eq. (44). It is worth noting that the fractal dimension of 1.67 is very close to that of aggregates formed in the diffusion-limited-cluster-aggregation (DLCA) regime, 1.7–1.8 [1,3,7,16].

Sorensen and Roberts [16] created 24 different aggregates in a three-dimensional space using a DLCA simulation and obtained the prefactor k_0 as a function of the fractal dimension D_f. From their work we take $k_0 = 1.60$ for $D_f = 1.67$, calculate $k_f = 0.83$ and $k_2 = 0.20$ using Eqs. (43) and (45), and obtain a corresponding value for the dimensionless hydrodynamic drag force (or radius) Ω of 0.59, which is visually indicated in Fig. 4.

Li and Logan [17] defined a settling velocity ratio, Γ, as

$$\Gamma = \frac{U}{U_s}, \tag{47}$$

where U and U_s, respectively, are the settling velocities of an aggregate and an impermeable sphere of the same mass within the common radius R. The bulk mass density of the impermeable sphere, ρ_b, is given as

$$\rho_b = \rho_p(1 - \epsilon) + \rho_f \epsilon, \tag{48}$$

where ρ_p and ρ_f are mass densities of the primary particle and fluid, respectively, and ϵ is the average porosity of the aggregate. In this case, one can easily find the following relationship between Γ and Ω:

$$\Gamma = \frac{U}{U_s} = \frac{(6\pi\mu RU)/F'}{(6\pi\mu RU_s)/F'} = \frac{\Omega^{-1}}{1} = \frac{1}{\Omega}, \tag{49}$$

where F' is the gravitational force subtracted by the buoyant force which is exerted on the impermeable sphere.

Then, we estimate a settling velocity ratio of our ideal aggregate to the impermeable sphere, 1.70, which is identical to that obtained using the cluster fractal model of Li and Logan [17] for large aggregates.

We also calculate a ratio of the hydrodynamic radius of Eq. (38) to the gyration radius of Eq. (42), given as

$$\frac{R_h}{R_g} = \Omega(k_2)\sqrt{\frac{D_f + 2}{D_f}}, \tag{50}$$

and obtain a value of 0.875, which is in excellent agreement with Chen et al.'s work [3]. They created 133 DLCA aggregates and obtained an R_h/R_g of 0.875 with $D_f = 1.78$, which is slightly higher than our fractal dimension of 1.67 but close enough within a few percentages of error.

3.2. Streamlines and fluid collection efficiency

The flow streamlines are shown in Figs. 5a and 5b for $k_2 = 0.20$ and $k_2 \to 0$, respectively. For $k_2 = 0.20$, some of streamlines near the vertical line passing through the center of the aggregate freely penetrate into the interior of the aggregate with significantly less flow deviation than those

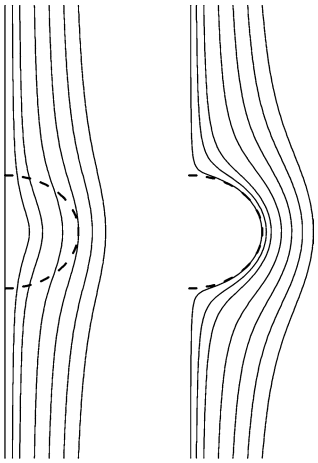

Fig. 5. Streamlines (a) inside and outside the ideal aggregate with $k_2 = 0.20$, and (b) outside the solid sphere (i.e., with $k_2 \to 0$).

detouring around the solid sphere. It visually implies that less hydrodynamic drag force is applied to the porous aggregate than is exerted on the solid sphere, implicitly confirming the Ω value of 0.59 (<1).

The fluid collection efficiency of the aggregate η can be defined as the ratio of the fluid passing through the aggregate to that approaching the aggregate within the cross-sectional area ($r < R$) [18]. A limiting streamline is defined as one that touches the aggregate at $r = R$ (or $\xi = 1$) and $\theta = \pi/2$, and so has a finite distance from the vertical line as $r \to \infty$. The corresponding mathematical description is

$$\eta = \lim_{r\to\infty} \frac{r^2 \sin^2\theta}{R^2} = \lim_{\xi\to\infty} \xi^2 \sin^2\theta. \tag{51}$$

Another definition of the fluid collection efficiency is the ratio of the fluid flow coming out of the upper hemisphere of the porous aggregate to that passing through an area of πR^2 at infinity, i.e.,

$$\eta = \frac{2}{V} \int_0^{\pi/2} u_r(R,\theta) \sin\theta \, d\theta. \tag{52}$$

The definitions of both Eqs. (51) and (52) yield an identical expression, given as

$$\eta = A + B + 1. \tag{53}$$

From Eq. (53), the value of η is calculated as 0.28 with the previously determined value of $k_2 = 0.20$. It is worth noting that Eq. (53) originates from the terms in the parentheses of Eq. (23) with $\xi = 1$.

4. Conclusion

An improved method of modeling the hydrodynamic properties of an ideal colloidal aggregate is derived in this study. The method recasts a fractal aggregate as a hydrodynamically equivalent sphere with quadratically increasing permeability from its center. The stream functions of fluid flow through the aggregate are then computed from the general analytical solution to the Brinkman and continuity equations. Further inspection of the fluid stream function reveals that the dimensionless hydrodynamic radius (or drag force) Ω is solely dependent on the permeability prefactor k_2. This implies that the hydrodynamic radius and settling velocity of an ideal aggregate are proportional to R and R^2, respectively, and that the fluid collection efficiency is not affected by the size of the aggregate. It is worth noting that the exponents of R in $U \propto R^2$, $R_H \propto R^1$, and $\eta \propto R^0$ are perfectly identical to those of an impermeable sphere.

Using Davies' permeability correlation (of Eq. (44)) and Sorensen and Robert's simulation result, the fractal dimension D_f and the permeability prefactor k_2 of the ideal aggregate are found to be 1.67 and 0.20, respectively. The values of D_f and k_2 well characterize DLCA aggregates in terms of their hydrodynamic radius and settling velocity. So, it can be inferred that the fluid collection efficiency of DLCA aggregates of fractal dimension of approximately 1.7 will reach as high as 0.28 regardless of the size of the aggregates.

Overall, an important conclusion drawn from this study is that an ideal aggregate exhibits a radially variable permeability that can be closely modeled as quadratically increasing from its core. The hydrodynamic behavior of a DLCA fractal aggregate can then be effectively modeled by this technique.

Acknowledgments

This work was supported in part by U.S. Geological Survey (Grant no. 01HQGR0079), through the Water Resources Research Center, University of Hawaii at Manoa, Honolulu. This is contributed paper CP-2005-03 of the Water Resource Research Center.

References

[1] P. Meakin, Adv. Colloid Interface Sci. 28 (1988) 249.
[2] M. Elimelech, J. Gregory, X. Jia, W. Williams, Particle Deposition and Aggregation: Measurement, Modeling, and Simulation, Butterworth–Heinemann, Oxford, 1995.
[3] Z.-Y. Chen, P. Meakin, J.M. Deutch, Phys. Rev. Lett. 59 (1987) 2121.
[4] S. Veerapaneni, M.R. Wiesner, J. Colloid Interface Sci. 177 (1996) 45.
[5] A.L. Chernyakov, J. Exp. Theor. Phys. 93 (2001) 771.
[6] C.P. Johnson, X. Li, B.E. Logan, Environ. Sci. Technol. 30 (1996) 1911.
[7] D.A. Weitz, M. Olivera, Phys. Rev. Lett. 52 (1984) 1433.
[8] A.S. Kim, K.D. Stolzenbach, J. Colloid Interface Sci. 253 (2002) 315.
[9] G. Ooms, P.F. Mijnlieff, H. Beckers, J. Chem. Phys. 53 (1970) 4123.
[10] H.C. Brinkman, Proc. K. Ned. Akad. Wet. (Amsterdam) 50 (1947) 618.
[11] H.C. Brinkman, Research (London) 2 (1949) 190.
[12] M. Vanni, Chem. Eng. Sci. 55 (2000) 685.

[13] S. Haber, R. Mauri, Int. J. Multiphase Flow 9 (1983) 561.
[14] J. Koplik, L. Herbert, A. Zee, Phys. Fluids 26 (1983) 2864.
[15] C.N. Davies, Proc. Inst. Mech. Eng. B 1 (1952) 185.
[16] C.M. Sorensen, G.C. Roberts, J. Colloid Interface Sci. 186 (1997) 447.
[17] X.-Y. Li, B.E. Logan, Wat. Res. 35 (2001) 3373.
[18] P.M. Adler, J. Colloid Interface Sci. 81 (1981) 531.